PHYSICAL REVIEW D **84,** 085029 (2011)

Can axionlike particles explain the alignments of the polarizations of light from quasars?

A. Payez,* J. R. Cudell,† and D. Hutsemékers‡
IFPA Group, AGO Dept., University of Liège, B4000 Liège, Belgium
(Received 11 July 2011; published 25 October 2011)

The standard axionlike particle explanation of the observed large-scale coherent orientations of quasar polarization vectors is ruled out by the recent measurements of vanishing circular polarization. We introduce a more general wave-packet formalism and show that, although decoherence effects between waves of different frequencies can reduce significantly the amount of circular polarization, the axionlike particle hypothesis is disfavored given the bandwidth with which part of the observations were performed. Finally, we show that a more sophisticated model of extragalactic fields does not lead to an alignment of polarizations.

DOI: 10.1103/PhysRevD.84.085029 PACS numbers: 14.80.Va, 95.30.Gv, 98.54.Aj

I. AXIONLIKE PARTICLES IN ASTROPHYSICS

A frequent prediction of extensions of the standard model of particle physics is the existence of stable weakly interacting light (sub-eV) scalar or pseudoscalar particles. The ''invisible'' axion [1–6] is certainly the best-known candidate, so that any particle of this kind is nowadays commonly referred to as an *axionlike particle* (ALP)—even though it might have nothing to do with the Peccei-Quinn solution to the strong *CP* problem [7]. Usually, the smallness of the masses of these particles is related to a very-high-energy scale where there would be new physics. Among these ALPs, one finds, for instance, chameleons, coming from $f(R)$ theories, but also scalar and pseudoscalar particles from Kaluza-Klein theories, superstrings, or other theories beyond the standard model, which could be testable predictions; for recent reviews, see for instance [8,9] and references therein.

The ALPs can have a coupling to photons, as is the case for the axion [10,11]. As the information we get from astrophysics comes mainly from photons from distant sources, this property makes them an appealing ingredient in many astrophysical models, and their existence could be probed by astrophysical observations. In fact, several authors have already reported different phenomena that might find a common explanation if one supposes the existence of nearly massless axionlike particles (of mass $m \leq 10^{-10}$ eV, and of coupling to photons $g \sim 10^{-11}$ GeV^{-1}), e.g. the transparency of the Universe to high-energy photons [12], the luminosity relations for active galactic nuclei (AGN) at different wavelengths [13], or the high-energy cosmic rays from blazars [14].

Another interesting observation has to do with the distribution of position angles for polarization of visible light coming from quasars.[1] These angles indicate the direction of maximum polarization for each source with respect to an arbitrary direction, usually the north equatorial pole. It has been reported that the distribution of these individual preferred directions in extremely large regions of the sky ($\sim$ Gpc) is not random [15–18]. From the latest sample available (355 quasars), global statistical tests indicate that the probability for the observed distribution to be random is between 3×10^{-5} and 2×10^{-3}, depending on the test applied [18]. This observation is remarkable as there is *a priori* no reason why one should expect such correlations over cosmological distances, larger than the most extended structures presently known in the Universe.

This analysis also indicates that the effect is not likely to be explained by local causes (influence of our galaxy, dust, etc.) and suggests that it requires something more exotic. One might think that it comes from an alignment of quasar axes across the Universe. It is known [19–22] that, for a given quasar, the direction of preferred polarization is related to its morphology, so that a global alignment of the axes of quasars would lead to aligned polarizations. On the other hand, if one supposes that the objects themselves are aligned, the effect should be present in radio waves. However, a study [20] based on a sample of 4290 objects (52 of them being part of the sample [18]) has shown that there is *no* evidence for alignments in radio waves. It thus seems that this class of explanations is disfavored.

On the other hand, it has been believed that these data could naturally be explained by the mixing of light with axionlike particles in background magnetic fields [23–31]: this would generate an alignment in visible light while leaving the polarization of radio waves unaffected, as the mixing depends on energy. In the present paper, we show that this requires a very specific choice of magnetic fields, and that in general the alignment effect cannot be explained by the mixing. Furthermore, we shall see that, according to recent data [32], the cause of this effect cannot be photon-ALP mixing, even for magnetic fields leading to an alignment.

*A.Payez@ulg.ac.be
†J.R.Cudell@ulg.ac.be
‡D.Hutsemekers@ulg.ac.be
[1]Hereafter, ''quasar'' stands for ''high-luminosity AGN.''

In the next section, we introduce our notations and recall results for the polarization of light described by plane waves due to the mixing of axionlike particles with photons. We then discuss why this cannot explain the data for the circular polarization of quasars and present a wave-packet treatment of the mixing in Sec. III. Our analysis shows that, despite promising phenomenological implications, even wave packets cannot reconcile the axionlike particle hypothesis with the full quasar sample. Further checks are made in Sec. IV, where we use different models for the magnetic field encountered by the incoming photons.

II. GENERALITIES, CONVENTIONS AND PLANE-WAVE FORMALISM

The mixing of photons with spin-0 particles ϕ changes the polarization of light because, in a background electromagnetic field, only one specific direction of polarization feels the interaction.

For pseudoscalars, the interaction Lagrangian contains a term proportional to $\phi(\vec{E}\cdot\vec{B})$. In our case, where we deal with external magnetic fields $\vec{\mathcal{B}}_e$, this reduces to $\phi(\vec{\mathcal{E}}_r\cdot\vec{\mathcal{B}}_e)$, with $\vec{\mathcal{E}}_r$, the electric field of the radiation from which the polarization is defined. Photons will thus mix with pseudoscalars through the projection of $\vec{\mathcal{B}}_e$ on their polarization vector. Things are similar for scalars [33], the main difference being that it is then the perpendicular direction which will mix, as the interaction is then related to $\phi(\vec{B}^2-\vec{E}^2)$, and the relevant term is $\phi(\vec{\mathcal{B}}_r\cdot\vec{\mathcal{B}}_e)$, with $\vec{\mathcal{B}}_r$ the magnetic field of the radiation, so that $\vec{\mathcal{E}}_r$ has to be perpendicular to $\vec{\mathcal{B}}_e$. We will now stick to what happens in the pseudoscalar case for the rest of the developments, bearing in mind that our results would also hold for scalars.

Strictly speaking, as they propagate, photons will in general have three polarizations because of the interaction with the electron plasma [34]. However, in our context, the longitudinal contribution is negligible as the electron density in the intergalactic medium is tiny. Hence it is sufficient to consider the projection of the magnetic field onto a plane perpendicular to the direction of propagation, i.e., the transverse part of $\vec{\mathcal{B}}_e$, noted $\vec{\mathcal{B}}$. We define an orthogonal basis made of the direction of propagation of light and of two directions $\vec{e}_\parallel$ and $\vec{e}_\perp$, parallel and perpendicular to the transverse field. Any light beam going in the z direction will then be written as $\vec{\mathcal{E}}_r(z,t)=\mathcal{E}_{r_\parallel}(z,t)\vec{e}_\parallel+\mathcal{E}_{r_\perp}(z,t)\vec{e}_\perp$.

We can now express the evolution of an electromagnetic wave in an external magnetic field $\vec{\mathcal{B}}$ and obtain the evolution of its Stokes parameters, due to the mixing with pseudoscalars. Stokes parameters are particularly interesting because they can fully describe the polarization of light, and because they are the quantities that observers directly measure, as they can be built out of intensities. We use the following definitions:

$$\begin{aligned} I(z) &= \langle \mathcal{I}(z,t)\rangle = \langle \mathcal{E}_{r_\parallel}\mathcal{E}^*_{r_\parallel}+\mathcal{E}_{r_\perp}\mathcal{E}^*_{r_\perp}\rangle,\\ Q(z) &= \langle \mathcal{Q}(z,t)\rangle = \langle \mathcal{E}_{r_\parallel}\mathcal{E}^*_{r_\parallel}-\mathcal{E}_{r_\perp}\mathcal{E}^*_{r_\perp}\rangle,\\ U(z) &= \langle \mathcal{U}(z,t)\rangle = \langle \mathcal{E}_{r_\parallel}\mathcal{E}^*_{r_\perp}+\mathcal{E}^*_{r_\parallel}\mathcal{E}_{r_\perp}\rangle,\\ V(z) &= \langle \mathcal{V}(z,t)\rangle = \langle i(-\mathcal{E}_{r_\parallel}\mathcal{E}^*_{r_\perp}+\mathcal{E}^*_{r_\parallel}\mathcal{E}_{r_\perp})\rangle. \end{aligned} \tag{1}$$

U and Q represent linear polarization, V the circular one and I the intensity; these quantities are averaged over the exposure time at a given distance z from the source. One often normalizes these parameters by the intensity I to enable comparisons between different sources (*e.g.*, $v=\frac{V}{I}$) and, as U and Q depend on the choice of axes, one also introduces the linear polarization degree and the polarization degree, respectively

$$p_{\rm lin}=\frac{\sqrt{Q^2+U^2}}{I} \quad \text{and} \quad p_{\rm tot}=\frac{\sqrt{Q^2+U^2+V^2}}{I}. \tag{2}$$

The parameters (1) have a property of additivity: a radiation described by a set (I, Q, U, V) can always be decomposed as the sum of two other ones, described by (I_1, Q_1, U_1, V_1) and (I_2, Q_2, U_2, V_2), as long as $I_1+I_2=I$, etc. In particular, a partially polarized beam can be described by the weighted sum of a fully polarized beam and of an unpolarized one: it is thus sufficient to discuss these two cases to obtain the most general case.

Formally, one can write a general initially fully polarized light beam of mean frequency ω and width $\Delta\omega$ as

$$\begin{aligned} \vec{\mathcal{E}}_r(z,t) = {}& \sin(\varphi_0)E_\parallel(z,t;\omega;\Delta\omega)\vec{e}_\parallel\\ & +\cos(\varphi_0)E_\perp(z,t;\omega;\Delta\omega)\vec{e}_\perp, \end{aligned} \tag{3}$$

where $E_\parallel\vec{e}_\parallel$ and $E_\perp\vec{e}_\perp$ are fully linearly polarized beams with polarizations, respectively, parallel and perpendicular to $\vec{\mathcal{B}}$, and with identical intensities. Initially, $E_\parallel$ and $E_\perp$ (which may differ by a phase shift) have the same behavior and shape, but this will change as they propagate. The angle φ_0 gives the initial direction of $\vec{\mathcal{E}}_r$. On the other hand, for an initially unpolarized beam, the Stokes parameters can be thought of as an incoherent average over φ_0 of the Stokes parameters of fully polarized beams.

The way the polarization parameters evolve in a magnetic field $\vec{\mathcal{B}}$ can be derived starting from a suitable Lagrangian density taking into account the interaction. For pseudoscalars, we use

$$\begin{aligned} \mathcal{L} = {}& \frac{1}{2}(\partial_\mu\phi)(\partial^\mu\phi)-\frac{1}{2}m^2\phi^2-\frac{1}{4}F_{\mu\nu}F^{\mu\nu}\\ & +\frac{1}{4}g\phi F_{\mu\nu}\tilde{F}^{\mu\nu}, \end{aligned} \tag{4}$$

where $\tilde{F}^{\mu\nu}\equiv\frac{1}{2}\epsilon^{\mu\nu\rho\sigma}F_{\rho\sigma}$ is the dual of the electromagnetic tensor, m is the pseudoscalar mass and g is the dimension-minus-one coupling constant of the interaction between pseudoscalars and photons.

At this stage, one can take into account plasma effects with the inclusion of the plasma frequency ω_p [35,36]:

$$\omega_p \equiv \sqrt{\frac{4\pi\alpha n_e}{m_e}} = \sqrt{\frac{n_e}{10^{-6}\ \mathrm{cm}^{-3}}} \times 3.7 \times 10^{-14}\ \mathrm{eV}, \quad (5)$$

which acts as an effective mass for the propagating electromagnetic field; n_e is the electron number density.

We first consider a constant magnetic field region in order to introduce the consequences of the mixing on polarization. We use in this case a typical field strength of 0.3 μG and a typical coherence scale of 10 Mpc, as in our supercluster [37–41], with an electron density such that $\omega_p = 3.7 \times 10^{-14}$ eV [24,37,40–42]. The equations for the electromagnetic potential and the pseudoscalar field are then found to be[2]:

$$\left[\left(\omega^2 + \frac{\partial^2}{\partial z^2}\right) - \begin{pmatrix} {\omega_p}^2 & 0 & 0 \\ 0 & {\omega_p}^2 & -g\mathcal{B}\omega \\ 0 & -g\mathcal{B}\omega & m^2 \end{pmatrix}\right] \begin{pmatrix} A_\perp(z) \\ A_\parallel(z) \\ \phi(z) \end{pmatrix} = 0, \quad (6)$$

for eigenstates of energy ω, in the timelike axial gauge $A^0 = 0$, so that $\vec{E}_{\perp,\parallel} = i\omega\vec{A}_{\perp,\parallel}$, and after a rephasing of $\phi(z)$. Note that Faraday rotation is not included in the discussion as its effect is irrelevant in the range of frequencies we are interested in.

The mass matrix in Eq. (6) is not diagonal, which means that $A_\parallel$ and ϕ are not the eigenmodes of propagation inside $\vec{\mathcal{B}}$. These are found by diagonalization and correspond to two new mass eigenvalues, μ_+ and μ_-, that depend on ω:

$${\mu_\pm}^2 = \frac{1}{2}({\omega_p}^2 + m^2) \pm r_{\mathrm{mix}}, \quad (7)$$

with

$$r_{\mathrm{mix}} \equiv \frac{1}{2}\sqrt{(2g\mathcal{B}\omega)^2 + ({m^2} - {\omega_p}^2)^2}, \quad (8)$$

and the mixing angle:

$$\theta_{\mathrm{mix}} = \frac{1}{2}\,\mathrm{atan}\left(\frac{2g\mathcal{B}\omega}{m^2 - {\omega_p}^2}\right). \quad (9)$$

For the moment, we always take $\phi(0) = 0$, i.e. we only consider incoming photons. The evolution of the Stokes parameters of Eq. (1) inside a magnetic field region for a plane-wave beam $\vec{\mathcal{E}}_r$ described initially by I_0, Q_0, U_0 and V_0 is given by[3]:

$$\begin{aligned} I(z) &= I_0 - \frac{1}{2}(I_0 + Q_0)\sin^2 2\theta_{\mathrm{mix}} \sin^2\left(\frac{1}{2}\frac{r_{\mathrm{mix}}}{\omega} z\right), \\ Q(z) &= I(I_0 \longleftrightarrow Q_0), \\ U(z) &= U_0\left\{(s_{\mathrm{mix}})^2 \cos\left((c_{\mathrm{mix}})^2 \frac{r_{\mathrm{mix}}}{\omega} z\right) + (c_{\mathrm{mix}})^2 \cos\left((s_{\mathrm{mix}})^2 \frac{r_{\mathrm{mix}}}{\omega} z\right)\right\} \\ &\quad - V_0\left\{(s_{\mathrm{mix}})^2 \sin\left((c_{\mathrm{mix}})^2 \frac{r_{\mathrm{mix}}}{\omega} z\right) - (c_{\mathrm{mix}})^2 \sin\left((s_{\mathrm{mix}})^2 \frac{r_{\mathrm{mix}}}{\omega} z\right)\right\} \mathrm{sign}(\theta_{\mathrm{mix}}), \\ V(z) &= U(U_0 \to V_0, V_0 \to -U_0), \end{aligned} \quad (10)$$

with $c_{\mathrm{mix}} \equiv \cos(\theta_{\mathrm{mix}})$ and $s_{\mathrm{mix}} \equiv \sin(\theta_{\mathrm{mix}})$. Hence, the evolution of Stokes parameters can be expressed in such a way that all the effects of the mixing with pseudoscalars in a given $\vec{\mathcal{B}}$ depend only on two dimensionless parameters: the mixing angle θ_{mix} and the quantity $(\frac{r_{\mathrm{mix}}}{\omega} z)$.

Equation (10) implies dichroism and birefringence; see, e.g. [26]. Dichroism is the selective absorption of one direction of polarization: it modifies the linear polarization of light. This effect is seen in the evolution of the Stokes parameter $Q(z)$ which compares the intensity in the two orthogonal directions. The total intensity $I(z)$ of course follows the same behavior. The pair (I, Q) is directly sensitive to the modifications of the amplitude of photons due to on-shell pseudoscalars.

Birefringence, on the other hand, indicates that linear and circular polarizations convert into each other. This strong connection between the two is explicit in the evolution of $U(z)$ and $V(z)$. The pair (U, V) is directly sensitive to the phase shift induced by virtual pseudoscalars: pure U requires a zero phase shift and pure V requires a $\frac{\pi}{2}$ phase shift between $\mathcal{E}_{r,\parallel}$ and $\mathcal{E}_{r,\perp}$.

Note that for an initially unpolarized light beam, while $I(z)$ and $Q(z)$ will evolve due to pseudoscalar-photon mixing, $U(z)$ and $V(z)$ will remain zero. The reason is clear: for unpolarized light, the concept of phase shift does not make sense. Similarly, if a linearly polarized beam points either exactly in the magnetic field direction or perpendicularly to it, i.e. $Q(0) \neq 0$ and $U(0) = 0$, there cannot be any induced phase shift and, therefore, no induced circular polarization.

[2]This is obtained to lowest order in $g\mathcal{B}$.

[3]The only simplification we have made to obtain Eq. (10) is to suppose $\omega^2 \gg \mu_\pm^2$, which indeed holds in all the applications we are interested in—as in most astrophysical situations where the mixing takes place in faint background magnetic fields.

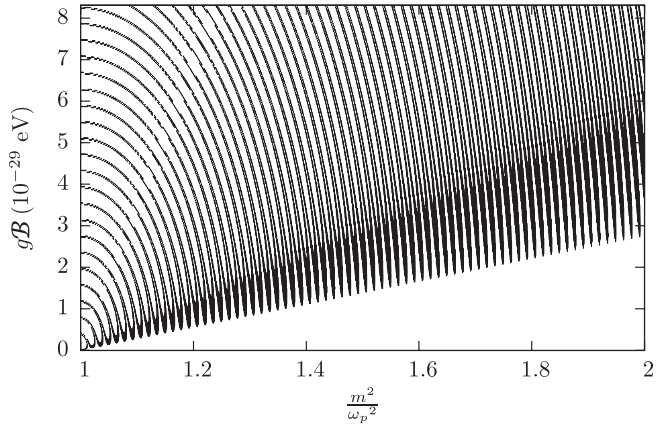

FIG. 1. Parameters such that the linear polarization generated through pseudoscalar-photon mixing in a transverse magnetic field region lies between 0.5 and 2% in the case of initially unpolarized light of wavelength $\lambda = 500$ nm. The magnetic field has been chosen to be 10 Mpc long; the plasma frequency is kept fixed at 3.7×10^{-14} eV.

A. Initially unpolarized light and dichroism

To reproduce coherent alignments of the polarizations of light from quasars, dichroism will be the main mechanism leading to the generation of a systematic amount of linear polarization: as estimated in [32], this has to be at least 0.5% and certainly not more than 2% to explain data. In order to present only this additional linear polarization, and avoid the arbitrariness of the initial one, we first consider unpolarized light beams.[4] For a given travelled distance z, and for a fixed value of ω_p, we study the space of parameters that reproduce the observed linear polarization. The result is shown in Fig. 1. Note that we do not display pseudoscalar masses smaller than ω_p since the linear polarization degree is an even function of $(m^2 - \omega_p^2)$. This remains true as long as there is no initial circular polarization.

What we learn from Fig. 1 is that, as long as m and ω_p are of the same order of magnitude, the mixing effect can in principle be observable and reproduce the observations, even in faint—but extended—magnetic fields ($\mathcal{B} = 0.1$ μG and $g = 10^{-11}$ GeV^{-1} correspond to $g\mathcal{B} = 1.95 \times 10^{-29}$ eV). The plasma frequency is very small in superclusters, and even smaller in cosmic voids, where only upper bounds exist to date in the literature [46–49]. With this scenario, the observations would then seem to be compatible with the existence of nearly massless axionlike particles. Note that the mixing depends on m and ω_p separately and that nothing special happens if we take $\omega_p = 0$.

[4]Note that even for partially linearly polarized light, which for quasars is at the 1% level [43–45], the unpolarized contribution will remain the dominant component.

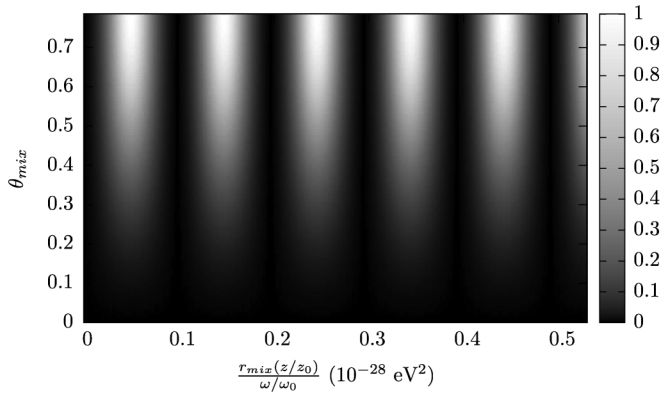

FIG. 2. Linear polarization degree (shown in the right-hand box) generated through pseudoscalar-photon mixing in a transverse magnetic field region in the case of initially unpolarized light. For convenience, we have introduced $\omega_0 = 2.5$ eV (i.e. $\lambda_0 = \frac{2\pi}{\omega_0} = 500$ nm) and $z_0 = 1.6 \times 10^{30}$ eV^{-1} ($\simeq 10$ Mpc).

For initially unpolarized light, the linear polarization degree (2) in terms of $\frac{r_{\rm mix}}{\omega} z$ and $\theta_{\rm mix}$ takes the form:

$$p_{\rm lin}(z) = \frac{\frac{1}{2}\sin^2 2\theta_{\rm mix}\sin^2[\frac{1}{2}\frac{r_{\rm mix}}{\omega} z]}{1 - \frac{1}{2}\sin^2 2\theta_{\rm mix}\sin^2[\frac{1}{2}\frac{r_{\rm mix}}{\omega} z]}. \tag{11}$$

We illustrate Eq. (11) in Fig. 2—strictly speaking $\theta_{\rm mix} \in [-\frac{\pi}{4}, \frac{\pi}{4}]$ but $p_{\rm lin}$ is an even function of it. Note that the maximum linear polarization is entirely determined by $\theta_{\rm mix}$, while the details of the oscillatory behavior with z are independently controlled by $r_{\rm mix}$. This can be physically understood as $\theta_{\rm mix}$ determines how much the particles mix, while $r_{\rm mix}$ has to do with the difference of mass eigenstates and is thus related to the wavelength of the oscillation. As long as the Lagrangian (4) makes sense, the oscillatory pattern in $\frac{r_{\rm mix}}{\omega} z$ repeats itself unchanged to infinity: all the physics can thus be studied in a small interval.

Now, if we are only interested in the parameters able to explain quasar linear polarization data, we get Fig. 3. We can also consider the average over one period in z of the additional polarization, and impose that it lies between 0.005 and 0.02. This gives an allowed range of values for $\theta_{\rm mix}$, which is

$$0.07 \leq |\theta_{\rm mix}| \leq 0.14. \tag{12}$$

B. Initially polarized light and birefringence

For astronomical sources, processes leading to the production of circularly polarized light are rare. Generally, most quasars only emit partially linearly polarized light; their polarization degree is typically around 1% [43–45]. In the following, we suppose that the initial distribution of polarization angles is random, so that the radiation can be described by random initial values for $q(0)$ and $u(0)$, with $p_{\rm lin}(0) = \sqrt{u^2(0) + q^2(0)} = 0.01$, and we assume no initial circular polarization: $v(0) = 0$. Note that the observed

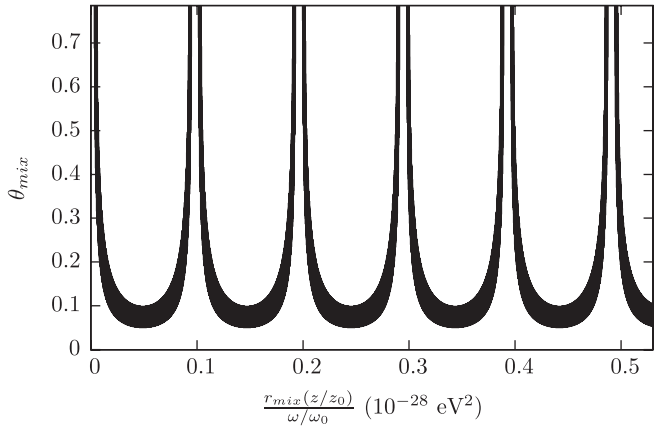

FIG. 3. Same as Fig. 2 but such that $p_{\rm lin} \in [0.005, 0.02]$. For fixed $z = z_0$ and $\omega = \omega_0$, this is equivalent to a reparametrization of Fig. 1.

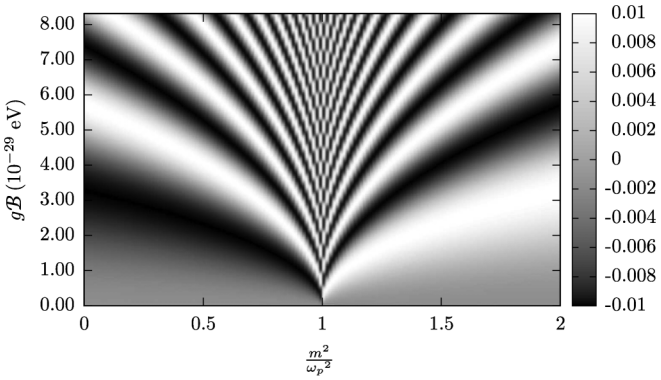

FIG. 4. Circular polarization v generated through pseudoscalar-photon mixing in a transverse magnetic field region, in the case of initially partially polarized light of wavelength $\lambda = 500$ nm with $u(0) = 0.01$. The plasma frequency and the size of the magnetic region are the same as in Fig. 1.

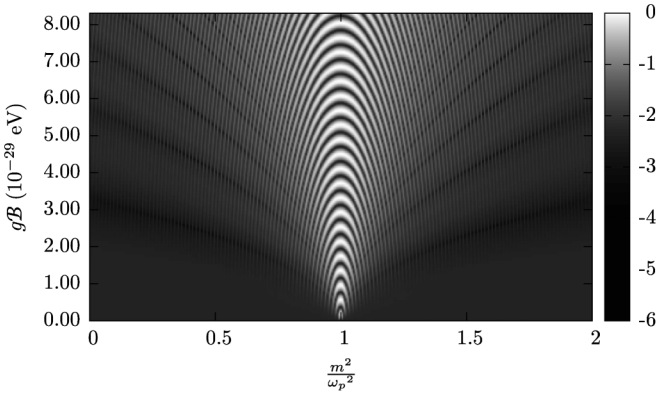

FIG. 5. Same as Fig. 4 but for the linear polarization degree. Note that the right-hand box gives the base-10 logarithm of the linear polarization.

linear polarization of the quasars in the sample is also of the order of 1%, and is believed to be mainly of intrinsic origin [15,16,18,45,50–52].

Now, while the mixing can generate enough linear polarization to reproduce the effect via axionlike particles, birefringence is expected to lead to an observable amount of circular polarization, see e.g. [11,32,53]. Indeed, as readily seen in Eq. (10), a linearly polarized light beam (with nonzero $u(0)$) will develop a circular polarization as it propagates.[5] From a technical point of view, an initial angle of $\frac{\pi}{4}$ with the direction of the external magnetic field leads to the maximal amount of generated circular polarization; it corresponds to $u(0) = p_{\rm lin}(0)$.

Moreover, even for light coming from a single quasar, a number of regions with different uncorrelated magnetic fields will be encountered on the way towards us. It is thus impossible to avoid $u(0) \neq 0$ at the beginning of some of these regions.

As we did for linear polarization in the initially unpolarized case, we now calculate the circular polarization v predicted by pseudoscalar-photon mixing when light is described by plane waves with $\lambda = 500$ nm, for an initial linear polarization of 1%. We show in Fig. 4 the circular polarization generated in one magnetic region, for $u(0) = p_{\rm lin}(0)$, and in Fig. 5 the corresponding linear polarization; as Stokes parameters are additive, any other case can be obtained from this one. Note that, as long as $v(0) = 0$, the circular polarization is an odd function of $(m^2 - \omega_p^2)$.

[5]This is also true for low-mass axionlike particles, even if the induced phase shift Φ drops quickly as the mass decreases: in the weak-mixing limit [54],

$$\Phi = \theta_{\rm mix}^2 \left[\frac{m^2 z}{2\omega} - \sin\left(\frac{m^2 z}{2\omega}\right) \right]. \quad (13)$$

In this astrophysical context, Φ is not small when the considered magnetic field regions are huge.

Figure 4 indicates that a large region of the parameter space leads to an observable circular polarization, i.e. most of the quasars should be circularly polarized, with a circular polarization of the order of the observed linear polarization.

III. NEW DATA ON CIRCULAR POLARIZATION AND DECOHERENCE

Recently, the circular polarization of quasars belonging to the sample [18] has been accurately measured in visible light. This analysis [32] shows that, except for two specifically highly polarized blazars, which might be intrinsically circularly polarized, the objects have a circular polarization consistent with zero.

This is clearly in contradiction with the results presented above for circular polarization; we show this in Fig. 6, in terms of $(\frac{r_{\rm mix} z}{\omega})$ and $\theta_{\rm mix}$. One sees that v is of the same order of magnitude as $p_{\rm lin}$, except in a small region (compare with Fig. 3): $\frac{r_{\rm mix}(z/z_0)}{(\omega/\omega_0)} \lesssim 0.2 \times 10^{-28}$ eV^{-2}, and $|\theta_{\rm mix}|$ with values similar to the ones in Eq. (12).

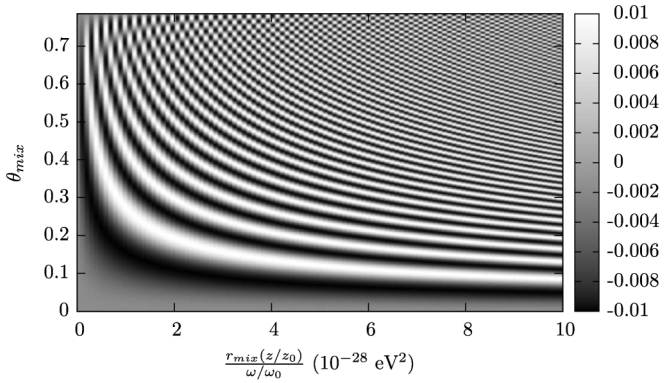

FIG. 6. Circular polarization v generated through pseudoscalar-photon mixing in a transverse magnetic field region in the case of initially partially polarized light with $u(0) = p_{\rm lin}(0) = 0.01$. The values of ω_0 and z_0 are the same as the ones introduced in Fig. 2.

Keeping an additional linear polarization of the order of 1% while suppressing the circular one then requires a considerable amount of fine-tuning of the masses, or smaller regions of magnetic field. The latter seems excluded as the correlations of polarizations over huge distances require magnetic fields to be coherent in large regions. To illustrate the need for fine-tuning, we can give a pseudoscalar mass for which enough linear polarization is created (the maximum of $p_{\rm lin}$ is determined by $\theta_{\rm mix}$), and such that the circular polarization is much smaller than the linear one (by choosing a suitable $r_{\rm mix}$).[6] First, we write the pseudoscalar mass as a function of $\theta_{\rm mix}$, and of $r_{\rm mix}$, for a fixed value of ω_p:

$$m = \sqrt{{\omega_p}^2 + 2r_{\rm mix}\cos(2\theta_{\rm mix})}, \quad \text{if} \quad m > \omega_p; \tag{14}$$

$$m = \sqrt{{\omega_p}^2 - 2r_{\rm mix}\cos(2\theta_{\rm mix})}, \quad \text{if} \quad m < \omega_p. \tag{15}$$

For $z = z_0 = 10$ Mpc and $\omega = \omega_0 = 2.5$ eV, $u(0) = 1\%$, and using $\theta_{\rm mix} = 0.1$, we then obtain that the only allowed ALP masses able to reproduce data would be such that:

$$\frac{m}{\omega_p} \in [0.99, 1.01]. \tag{16}$$

This is a very fine-tuned situation, especially given that we have allowed v to be as large as 0.1% in this example.[7] Note also that the plasma frequency is expected to vary along the light trajectory, so that (16) cannot be maintained. These data thus disfavor the ALP hypothesis in the plane-wave case.

[6]We can consider $\theta_{\rm mix}$ as determined in the unpolarized case: the additional polarization will indeed not be very different here, as by requiring no v, we essentially constrain u not to change.

[7]If we require $v < 0.01\%$, the range of allowed values for the mass shrinks to $m \in [0.998, 1.002]\omega_p$.

A. A wave-packet treatment

We now consider the possibility of reducing circular polarization by considering wave packets, which automatically include the possibility of decoherence between waves of different frequencies. As circular polarization is a matter of phase shifts, decoherence effects can significantly reduce it. There is also a natural observational reason for taking into account this effect: astronomers perform polarimetric measurements in given ranges of frequencies, with given filters. In the case at hand, some data were obtained in white light (unfiltered), and some with the so-called "Bessell V-filter" [55,56].

From the Lagrangian (4), the system of relevant equations is

$$\begin{aligned}(\Box + {\omega_p}^2)E(z,t) - g\mathcal{B}\partial_t^2\phi(z,t) = 0\\ (\Box + m^2)\phi(z,t) + g\mathcal{B}E(z,t) = 0,\end{aligned} \tag{17}$$

where we simplify the notation: from now on, $E \equiv E_\parallel$. Note that the solution for $E_\perp$ will simply be that for $E_\parallel$, with $g\mathcal{B}$ set to zero.

We consider the case in which a wave packet is sent into a region of constant magnetic field $\mathcal{B}$, starting at $z = 0$, and use wave packets in ω:

$$\begin{aligned}E(z,t) &= \int_{-\infty}^{\infty} d\omega\; e^{-i\omega t}\tilde{E}(z,\omega) \quad \text{and}\\ \phi(z,t) &= \int_{-\infty}^{\infty} d\omega\; e^{-i\omega t}\tilde{\phi}(z,\omega).\end{aligned} \tag{18}$$

Equations (17) have then to be satisfied by the integrands of (18) in each region, with $\mathcal{B} = 0$ if $z \le 0$ (region I), and $\mathcal{B} \neq 0$ if $z \ge 0$ (region II); the solutions are given in Appendix A. For the rest of the discussion, the incident packet in the first region has the initial shape

$$\tilde{E}_{i,I}(z = 0, \omega) = e^{-(a^2/4)(\omega-\omega_0)^2}. \tag{19}$$

1. Size of the wave packets

Continuum light coming from quasars, at least in UV and visible wavelengths, is thermally emitted in the accretion disk. In order to obtain an estimate of the wave-packet size in this case, we can start with results for blackbody radiation: we decompose the accretion disk into a concentric collection of black bodies of different temperatures at different radii [57,58].[8] For a blackbody radiation of Wien wavelength λ_w, estimates of the longitudinal coherence length l_c have been obtained in interferometry [59]: $l_c \simeq \lambda_w \simeq \bar{\lambda}$, with $\bar{\lambda}$, the mean wavelength of the radiation. The relation that we use for the value of a which enter Eq. (19) is then[9]

[8]Strictly speaking, one would then have to average the results obtained for different blackbodies over the range of frequencies actually observed.

[9]From [59], this can change slightly, depending on the definition of the full-width-at-half-maximum in frequencies.

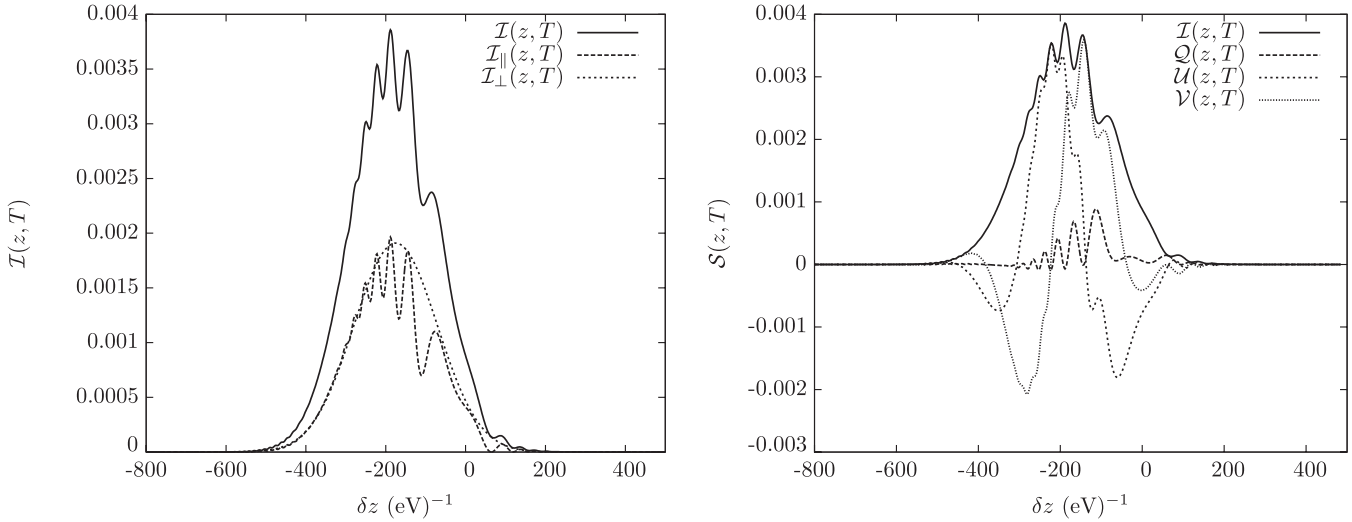

FIG. 7. The shape of the wave packets at time $T = 10$ Mpc$/c$ for a light beam with $u(0) = 1$. The abscissa is $\delta z \equiv z - cT$, which is the shift in position with respect to a frame moving at the speed of light c; i.e. here the origin is at 10 Mpc. *Left*: we show the total intensity and the intensities for the polarizations parallel and perpendicular to the magnetic field, before integration. *Right*: we show the contributions to the other Stokes parameters. We used $\omega_p = 3.7 \times 10^{-14}$ eV, $m = 4 \times 10^{-14}$ eV, $\omega_0 = 2.5$ eV (i.e. $\lambda_0 = 500$ nm), $a = 1.34$ eV^{-1}, and $g\mathcal{B} = 3 \times 10^{-29}$ eV.

$$a = \frac{2\sqrt{\ln(2)}}{\pi}\bar{\lambda}, \tag{20}$$

and the initial full-width at half-maximum in position is

$$\Delta z \simeq \sqrt{2\ln(2)}a, \tag{21}$$

which is thus of the order of the wavelengths considered.

2. Stokes parameters and partially polarized light

As wave packets go through the detector much faster than its time resolution, one has to integrate the packets over the exposure time Δt to calculate the Stokes parameters. Let us now represent by S any of the four Stokes parameters; with the notations of Eq. (1), the observed quantities are then

$$S(z) = \langle \mathcal{S}(z,t)\rangle \equiv \frac{1}{N^2}\int_t^{t+\Delta t} dt\, \mathcal{S}(z,t), \tag{22}$$

where we introduce the normalization[10] constant $N = (2\pi)^{-3/4}\sqrt{a}$, which cancels in polarization degrees and normalized Stokes parameters. In Fig. 7, we illustrate the packets after a propagation inside region II in a strong mixing case.[11] For photon polarizations parallel to $\vec{\mathcal{B}}$ we see the effect of interferences within the packet, while there is only a spread for nonmixing photons. Note that this is for 100% polarized light, so that the obtained $U(z)$ and $V(z)$ are much larger than what the same conditions would give for typical quasars light. Now we need a correct description of what happens to initially unpolarized and partially linearly polarized light described with wave packets.

To treat partially polarized light, one can make use of a useful property of Stokes parameters in the case of fully polarized light, defined as in Eq. (3). For fixed external conditions, calculating Stokes parameters in the $\varphi_0 = \frac{\pi}{4}$ case gives us access to the following quantities:

$$\begin{aligned}
Q_{\rm pol}\left(z;\varphi_0 = \frac{\pi}{4}\right) &= \left\langle \frac{1}{2}(|E_\perp|^2 - |E_\parallel|^2)\right\rangle \equiv C_1(z),\\
I_{\rm pol}\left(z;\varphi_0 = \frac{\pi}{4}\right) &= \left\langle \frac{1}{2}(|E_\perp|^2 + |E_\parallel|^2)\right\rangle \equiv C_2(z),\\
U_{\rm pol}\left(z;\varphi_0 = \frac{\pi}{4}\right) &= \langle 2\,{\rm Re}\{E_\parallel E_\perp^*\}\rangle \equiv C_U(z),\\
V_{\rm pol}\left(z;\varphi_0 = \frac{\pi}{4}\right) &= \langle 2\,{\rm Im}\{E_\parallel E_\perp^*\}\rangle \equiv C_V(z),
\end{aligned} \tag{23}$$

which evolve with z due to the mixing with pseudoscalars. One can easily show that the evolution of the Stokes parameters for any other light beam $\vec{\mathcal{E}}_r$, with initial angle φ_0, in the same conditions is

$$\begin{aligned}
I_{\rm pol}(z;\varphi_0) &= C_1(z)\cos(2\varphi_0) + C_2(z),\\
Q_{\rm pol}(z;\varphi_0) &= C_2(z)\cos(2\varphi_0) + C_1(z),\\
U_{\rm pol}(z;\varphi_0) &= C_U(z)\sin(2\varphi_0),\\
V_{\rm pol}(z;\varphi_0) &= C_V(z)\sin(2\varphi_0),
\end{aligned} \tag{24}$$

i.e. it is sufficient to calculate the coefficients (23).

[10]This value of N corresponds to an initial intensity of 1 eV^4.
[11]We use the Multiple-Precision Floating-point library with correct Rounding [60].

Now, as we have already discussed, unpolarized light can be thought of as the average over every possible initial angle φ_0. Applied to Eq. (24), this averaging gives, for unpolarized light: $I_{\rm unpol}(z) = C_2(z)$, $Q_{\rm unpol}(z) = C_1(z)$ and $U_{\rm unpol}(z) = V_{\rm unpol}(z) = 0$.

The evolution of any Stokes parameter S for a light beam initially with a partial linear polarization, characterized by a given value of $p_{\rm lin,0}$ and a value of φ_0, then follows:

$$S_{\rm partial}(z;\varphi_0, p_{\rm lin,0}) = p_{\rm lin,0} S_{\rm pol}(z;\varphi_0) + \frac{1}{2\pi}\int_0^{2\pi}(1 - p_{\rm lin,0}) S_{\rm pol}(z;\varphi) d\varphi. \tag{25}$$

This finally leads to a natural generalization of the fully polarized case:

$$\begin{aligned} I_{\rm partial}(z;\varphi_0, p_{\rm lin,0}) &= p_{\rm lin,0}[C_1(z)\cos(2\varphi_0)] + C_2(z), \\ Q_{\rm partial}(z;\varphi_0, p_{\rm lin,0}) &= p_{\rm lin,0}[C_2(z)\cos(2\varphi_0)] + C_1(z), \\ U_{\rm partial}(z;\varphi_0, p_{\rm lin,0}) &= p_{\rm lin,0}[C_U(z)\sin(2\varphi_0)], \\ V_{\rm partial}(z;\varphi_0, p_{\rm lin,0}) &= p_{\rm lin,0}[C_V(z)\sin(2\varphi_0)]. \end{aligned} \tag{26}$$

B. Results for white light

We now present the results of the mixing of photons with axionlike particles in a wave-packet formalism. We shall argue that these packets can be used to describe white light, with no photometric filter. The photomultipliers used to perform the white-light measurements of polarization have a broad spectral-response range (from 185 to 930 nm for the ones used in [61]), which is indeed similar to the width of our wave packets.

Note that current upper limits on the pseudoscalar[12] coupling are $g = 10^{-11}$ GeV^{-1}. Together with $\mathcal{B} = 0.3$ μG, this means that $g\mathcal{B} \lesssim 6 \times 10^{-29}$ eV.

In Fig. 8, we first illustrate the different Stokes parameters at a given distance, for each initial value of the angle φ_0. For a given angle, the distance between the origin and each $S(z;\varphi_0)$ curve is the value of this Stokes parameter. Now, for wave packets, we obtain that the circular polarization $V(z)$ is strongly reduced with respect to the plane-wave prediction; notice that $U(z)$ is also affected in the same way, as it is also very sensitive to phase effects. This can be understood if one goes back to Fig. 7: we see that these two quantities change sign within the packet itself, due to the extremely frequency-dependent character of the birefringent effect induced by the pseudoscalars. Also note that, whereas for plane waves the Stokes parameters obey $I^2(z) = Q^2(z) + U^2(z) + V^2(z)$ for any φ_0, this is no longer true in the wave-packet case, even for light initially fully linearly polarized.

[12]Interestingly, for chameleons constraints are even less severe [13].

For partially polarized light the expected amount of circular polarization will of course be even smaller. This is shown in Figs. 9 and 10, which are the wave-packet results analogous to those of the plane-wave case (Figs. 4 and 5). We obtain a large suppression of circular polarization for most of the parameters. Let us emphasize that this is in the case leading to the highest amount of v; i.e. $u(0) = p_{\rm lin}(0) = 0.01$. Besides, notice that the maximum linear polarization attainable for some of the parameters is smaller than in the plane-wave case: this is related to the loss of u that happens in this case, as also seen in Fig. 8.

In Fig. 11, we also directly compare the two descriptions for different values of the coupling; one can see that, for very small $g\mathcal{B}$, the results are similar, and that the suppression is more efficient at larger values of $g\mathcal{B}$.

Finally, we have generalized our calculations to the case where the packets are initially described by the frequency distribution (19), somewhere in the first region, at some $\tilde{z} \ll 0$. The first region can then represent a cosmic void, where ω_p can also typically have a smaller value; this allows the packet to propagate a long time, which makes it spread, before it enters the second region. We have checked that the results we have presented above hold in this case as well (even if the first region is taken to be one gigaparsec long). This confirms that the main mechanism that reduces the circular polarization is not related to the separation and the spread of photon packets of different polarization, but rather because of phase shifts within the packets that mix. This can be understood as $v(\omega)$ can change sign within the packet, averaging to zero, while $p_{\rm lin}(\omega) = \sqrt{q^2(\omega) + u^2(\omega)}$ cannot, keeping an alignment possible.

A simpler approach [62] is to use direct averages of the plane-wave Stokes parameters of Eq. (10) over frequency, instead of wave packets. This will give the same qualitative results, as illustrated in Fig. 12, where quantities are plotted against $\Delta\omega$, the bandwidth over which each averaging is performed. For the averages of plane waves, we have used the analytical formulas (10) averaged over a step profile in ω, centered around ω_0 and of width $\Delta\omega$. For the Gaussian wave packets of Eq. (19), on the other hand, we chose $\Delta\omega$ to represent the full-width-at-half-maximum in ω of each initial packet (i.e, $a = 4\sqrt{\ln(2)}(\Delta\omega)^{-1}$). In either case, the larger the band of frequencies over which the averaging is done, the smaller the absolute value of the circular polarization and its relative importance compared to the linear polarization. This holds whatever the details of the averaging. Similar results have also been obtained in different contexts (chameleons [40], and high-energy gamma sources [63]).

Therefore, as far as white-light data are concerned, phenomenological implications of axionlike particles mixing with photons can be reconciled with circular polarization measurements [28–30].

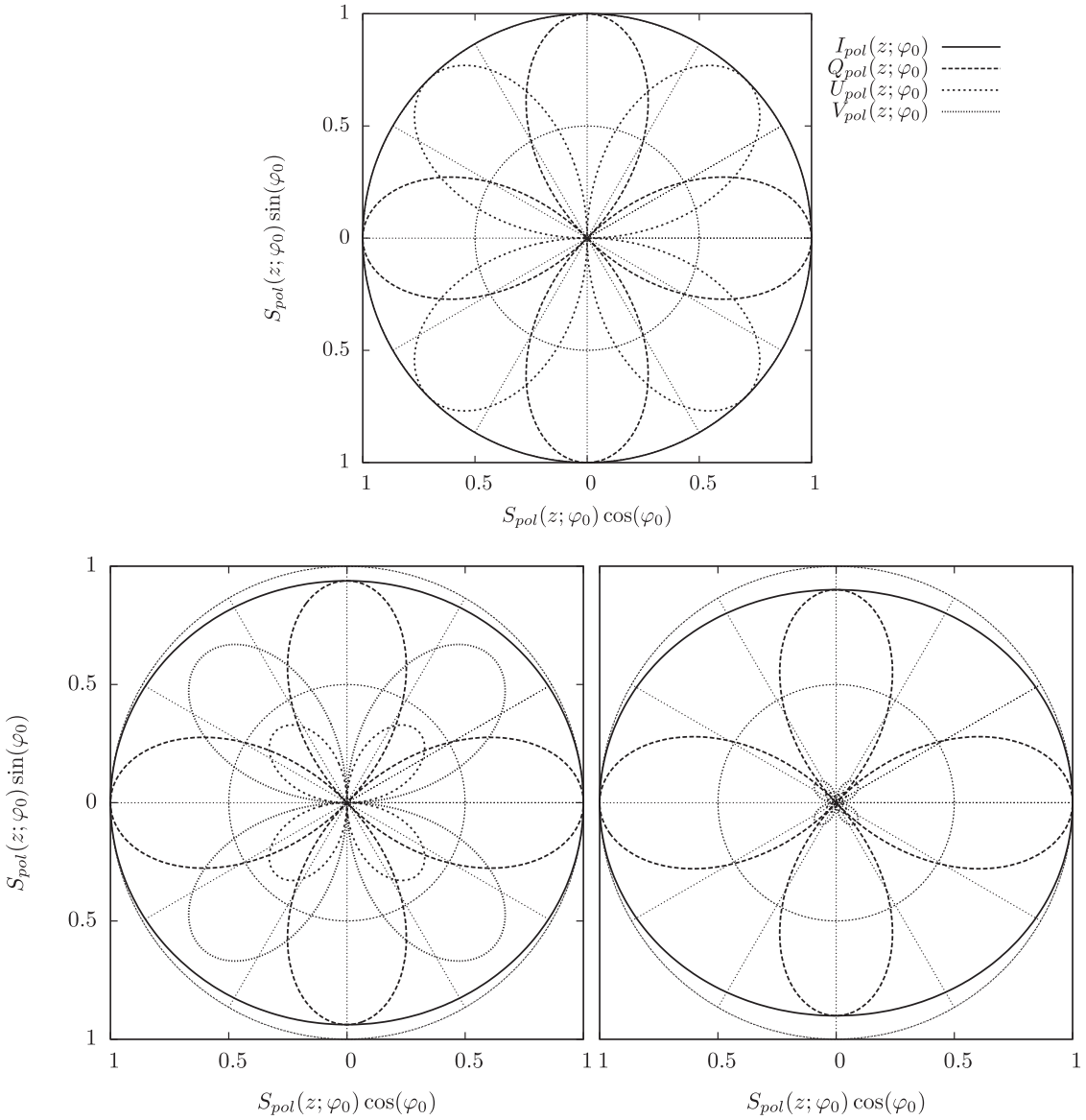

FIG. 8. Stereographic views of each of the Stokes parameters before (*top*), and after a 10 Mpc propagation inside a magnetic field with plane waves (*bottom left*), and with wave packets (*bottom right*), for initially 100% linearly polarized light. The distance of the curves to the origin gives the value of the parameters. To enable direct comparisons, the angular coordinate in the three figures is the initial angle, φ_0. The direction of the magnetic field is the one given by $\varphi_0 = \pm\frac{\pi}{2}$. This relatively strong mixing case is shown for $m = 4.5 \times 10^{-14}$ eV, $\omega_p = 3.7 \times 10^{-14}$ eV, $g\mathcal{B} = 5 \times 10^{-29}$ eV, $\omega_0 = 2.5$ eV, and $a = 1.34$ eV^{-1}.

C. Results for Bessell V-filter

Most of the recent circular polarization data of [32] were taken using a Bessell broadband V filter [55,56]. This filter is centered around $\lambda = 547.6$ nm and the associated full-width-at-half-maximum is 113.2 nm. To mimic this cut in frequencies, one can convolute wave packets with the spectrum distribution of the filter, or proceed to averages of plane-wave results over ω using the frequency profile.

We then find that, even though it is a broadband filter, the typical values of the astrophysical parameters are such that the circular polarization does not change sufficiently over this bandwidth to be strongly reduced when averaging over ω. This is illustrated in Fig. 12 for small values of $\Delta\omega$ (≈ 0.5 eV). The circular polarization is slightly smaller than in the monochromatic case, but the effect is certainly not sufficient to reconcile the mechanism with the data. Except for very specific choices of parameters, the axionlike-particle parameters able to create an alignment will also predict a sizeable amount of circular polarization.

If axions were at work, given the—somehow narrow—bandwidth of the broadband V-filter, circular polarization

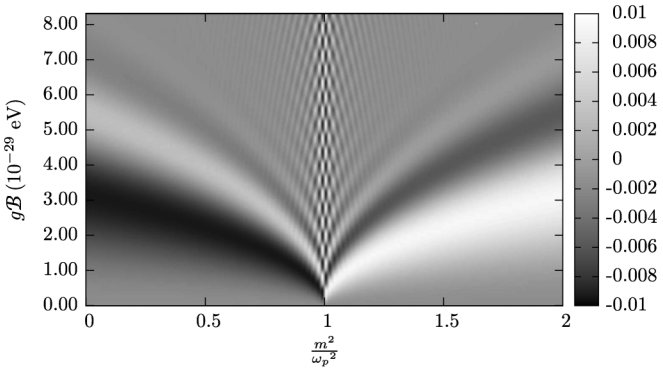

FIG. 9. Same (circular polarization) as Fig. 4 but with light described by wave packets. We have used $\omega_0 = 2.5$ eV and $a = 1.34\ \text{eV}^{-1}$.

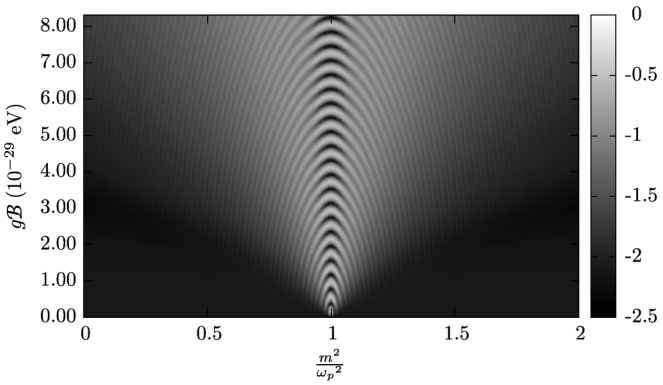

FIG. 10. Same (linear polarization) as Fig. 5 but with light described by wave packets. We have used $\omega_0 = 2.5$ eV and $a = 1.34\ \text{eV}^{-1}$. Note that the right-hand box gives the base-10 logarithm of the linear polarization.

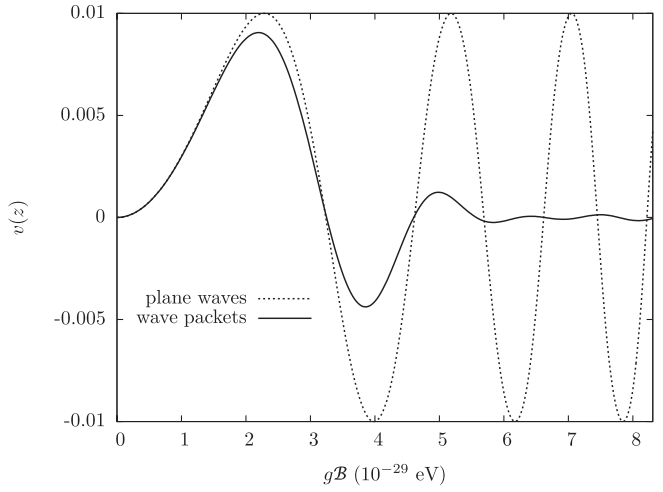

FIG. 11. Comparison of results obtained with plane waves and with wave packets, for the same parameters. This is a cut, respectively of Fig. 4 and of Fig. 9, for the pseudoscalar mass $m = 4.5 \times 10^{-14}$ eV.

should have been observed, even with a wave-packet description.

IV. DIFFERENT MODELS FOR THE MAGNETIC FIELD

We are going to focus on the regions where these V-filter data have been taken from and check the sensitivity of the result to changes in the magnetic field morphology. We will see that the mixing with pseudoscalars in a magnetic field that fluctuates along the light trajectory cannot even reproduce the alignments of linear polarization.

A. Linear polarization data towards region A1

In order to detect alignments, we shall first argue that averages in the (q, u) space give the same information as the more elaborate methods of [18].

Among quasars with circular polarization measured in the V-filter, 18 are located in the same direction of the sky, towards what is called region A1 in [15,16,18]. We can present in a (q, u) space the linear polarization of quasars located in this direction,[13] and see what the alignment effect looks like in such a plot. As the polarization angle is related to the Stokes parameters q and u via the relation:

$$\varphi = \frac{1}{2}\,\text{atan}\left(\frac{u}{q}\right), \tag{27}$$

for a fixed value of p_{lin} different values of q and u correspond to different orientations. In particular, a random distribution of polarization angles corresponds to an isotropic distribution in this space. Note also that, as $p_{\text{lin}} = \sqrt{q^2 + u^2}$, the distance between the origin and a given point directly gives the degree of polarization of the associated light beam.

In Fig. 13, we show data from the latest sample [18], for both low- and high-redshift quasars.[14] As expected, coherent orientations are translated into departures from isotropy in such a graph. Note that the preferred direction for the asymmetry is not the same for low and high redshifts, while these objects are along the same line of sight.

To be more quantitative, we can calculate the mean values of q and of u, for low- and high-redshift data, taking into account the experimental uncertainties.[15] We determine the mean values and the errors on the mean for q and u and plot them in Fig. 13; we obtain $(-0.0135 \pm 0.0072,\ 0.0041 \pm 0.0039)$ for the low-redshift region, and $(0.0097 \pm 0.0035,\ -0.0019 \pm 0.0041)$ for the high-redshift one. In the observational paper [18], another analysis was done: they obtained the preferred angles one finds

[13]Doing so, we drop the information about the position of each object on the sky.

[14]Only objects with $p_{\text{lin}} \geq 0.6\%$ have been considered in this sample, this is why there is a hole in the center of those figures.

[15]For this, one takes $\sigma_q = \sigma_u = \sigma_p$, see Ref. [64].

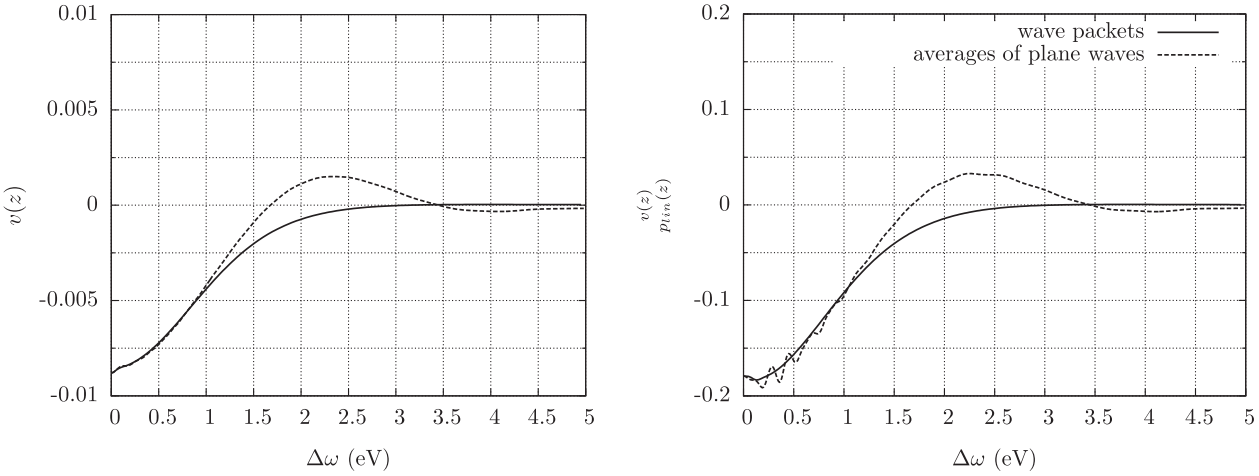

FIG. 12. Comparing averaging methods for wave packets (with $a = \frac{4\sqrt{\ln(2)}}{\Delta\omega}$) and averages of plane waves: in both cases, the absolute values of υ (*left*) and of $\frac{\upsilon}{p_{\rm lin}}$ (*right*) are reduced with increasing $\Delta\omega$ with respect to the monochromatic case (i.e. $\Delta\omega = 0$). Here, we used $g\mathcal{B} = 6 \times 10^{-29}$ eV, and $\Delta\omega$ is centered around $\omega_0 = 2.5$ eV; the other parameters are the same as in Fig. 11.

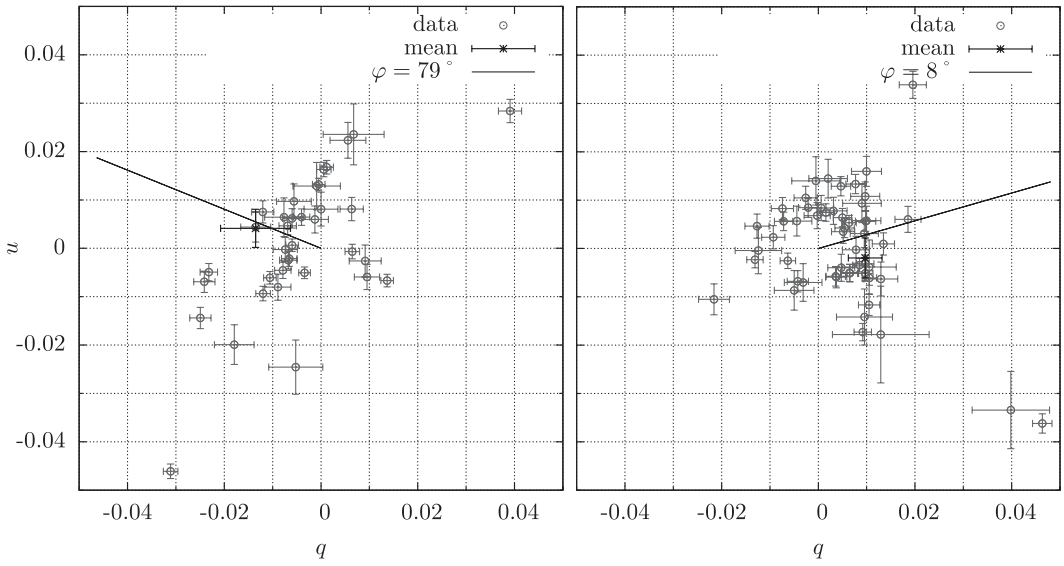

FIG. 13. Experimental data: objects taken in the A1 direction. *Left*: linear polarization for low-redshift quasars, with $0 \leq z < 1$. *Right*: same for high-redshift ones, with $1 \leq z \leq 2.3$. Some objects with higher polarization degrees are not shown, but are taken into account for the mean. In the case of low-redshift quasars, the total number of objects is $N = 43$, and for high-redshift ones, it is $N = 56$.

when considering only the angular information; these are shown with straight lines.

B. Models

The location of region A1 points towards the center of the Virgo supercluster (our local supercluster, shortened as "LSC"). To the best of our knowledge, the Virgo magnetic field can be described either [38,41]:

(i) by a uniform field (used thus far for illustration) with a magnitude $\approx$ 0.2–0.3 μG over $\approx$ 5–10 Mpc;
(ii) by a "patchy" field made of several $\approx$ 100 kpc cells of randomly oriented magnetic field of strength ≈ 2 μG, adding up to the same distance.

Note that a "patchy" picture is also typically what is considered to discuss the propagation of cosmic rays, and what is obtained from structure formation; see for instance [65,66] for results about the LSC.

The LSC magnetic field is essentially the last relevant magnetic field encountered by extragalactic photons coming towards us.[16] For this reason, regardless of its structure, the axionlike particle explanation of quasar data will be

[16]The influence of our galactic magnetic field can be neglected: the field strength decreases exponentially in the direction transverse to the galactic plane [39], and data have been obtained at high galactic latitudes.

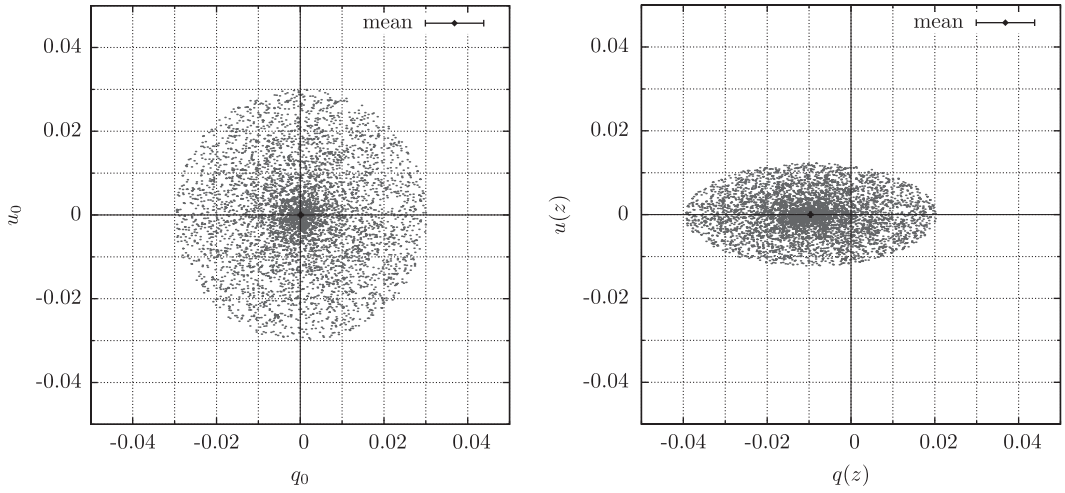

FIG. 14. 5000 beams are generated. *Left*: initial distribution. *Right*: The associated distribution after effects induced by axion-photon mixing in the uniform case. The parameters used here are $\omega_0 = 2.25$ eV, $\omega_p = 3.7 \times 10^{-14}$ eV, $m = 4.5 \times 10^{-14}$ eV, $g = 3.5 \times 10^{-12}$ GeV^{-1}, $\mathcal{B} = 0.3$ μG, and $z = 10$ Mpc.

ruled out if the influence of this field creates too much circular polarization, as any v created there should have been detected.

1. Simulations in the uniform-field scenario

We know since Sec. III C that a uniform field can produce coherent orientations of polarization with respect to the magnetic field direction, although the existence of axionlike particles responsible for an alignment would have also implied that circular polarization is produced. As we have discussed, this is excluded by data.

We can check what this alignment looks like in a (q, u) space, if we start from a random distribution of polarization.

To mimic a random distribution of initial quasar polarizations, we first generate partially polarized light beams ($p_{\rm lin}$ between 0 and 3%), with random polarization angles. In Fig. 14, on the left, we plot this initial distribution of light beams, each random realization being displayed using its Stokes parameters q and u. On the right, we show what this distribution becomes, due to axion-photon mixing inside the 10 Mpc uniform magnetic field. We see that there is indeed a departure from a random distribution acquired through the mixing, corresponding to an asymmetry in the (q, u) space.[17] More quantitatively, the means we obtain for q and u in this example lead to a value of $p_{\rm lin} = 0.01$ after axion-photon mixing, while they were compatible with zero initially.

2. Simulations in the patchy scenario

Pure randomness—As already mentioned, making the magnetic field fluctuate in a ''patchy'' model may suppress v: as we have seen in Sec. III, in small-enough magnetic-field regions, the induced circular polarization can be smaller than the linear one. Nevertheless, circular polarization is not the main problem in this picture.

Indeed, it is obvious that such a field will not help create an alignment: if the magnetic field can be thought of as small cells with magnetic field directions distributed in a random way from cell to cell, this will be the case along the line of sight, but also transversally. Then, two objects which are angularly separated will pass through two different magnetic field configurations. There is thus no way to create an alignment, as there is no preferred direction in this problem that is common to all quasars.

With an underlying uniform field—We can go further and use a more refined model, where there would be at least some correlation between the cells rather than a complete randomness. To do this, we sum the magnetic fields of the uniform and of the ''patchy'' models, using results presented in Appendix B. We thus have cell-like magnetic fields on top of a fainter field, this one being coherent over the LSC scale: this would lead to some semirandomness between the cells on the LSC scale, as discussed in [38].

In this case, to keep a final linear polarization of the order of 1%, we have to consider either smaller values of the coupling, or bigger values of $|m^2 - {\omega_p}^2|$ than in the uniform case because the magnetic field is stronger (see Eq. (9)).

For this reason, and because the field strength of the uniform component is ≈ 7 times smaller than that of the randomly oriented one, it is not surprising that there is no obvious departure from isotropy due to axion-photon mixing in this case. Indeed, the effect induced by the uniform component of the magnetic field is then strongly suppressed: therefore, an alignment cannot be achieved. For the example we present in Fig. 15, we obtain that the means

[17]The fact that the asymmetry appears along one of the axes is only due to our specific choice for the basis; only $p_{\rm lin}$ is a physical quantity.

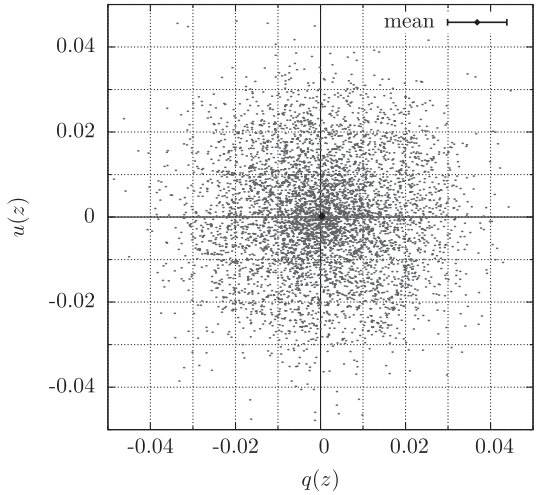

FIG. 15. Same as Fig. 14 (*right*) but after axion-photon mixing in the "patchy" case with an underlying uniform field. The parameters used here are the same as before, except $m = 1.85 \times 10^{-13}$ eV. For the uniform magnetic field, we use $\mathcal{B} = 0.3\ \mu$G over 10 Mpc; for the randomly oriented part of the magnetic field, we use $|\vec{\mathcal{B}}_c| = 2\ \mu$G in a hundred 100 kpc-long cells.

of q and u are compatible with zero at the 1σ-level, namely, hardly any improvement with respect to the initial distribution, and certainly not enough additional linear polarization to be able to explain the data. We checked that if the relative intensities of the random and background fields are chosen to produce an alignment, then the circular polarization is again too high.

If this second possibility turns out to be a satisfactory model of the magnetic field of the local supercluster, not only would there be some circular polarization, but axionlike particles will be unable to create coherent orientations in that field. Note that these results are general and do not only apply to the LSC magnetic field.[18]

Finally, we have also checked that our results are stable with respect to fluctuations of a factor of 2 (up or down) of the parameters, among which the plasma frequency, the cell sizes, and the magnetic field strength.

V. CONCLUSION

In this paper, we have considered photon-pseudoscalar mixing as the source of the observed alignments. This process has so far been the best hope to explain the observed data. The typical treatment assumes that the same faint coherent field is traversed by the light beams from all the quasars. Note that this is problematic, as the data display two alignments: quasars at redshift $z > 1$ seem to be aligned in a different direction from closer ones. In order to obtain such an effect, one needs to assume a slice of coherent fields 1 Gpc large, with an intensity of the order of 0.1 μG. Although this seems unlikely, one cannot rule out the explanation on those grounds, as so little is known about magnetic fields at high redshifts.

Recent data have shown that the circular polarization of these objects is negligible, contrarily to the predictions from photon-pseudoscalar mixing. At face value, this kills the interpretation. However, we showed that it is possible to argue that, for white light, the average over frequencies suppresses the circular polarization enough. From the sample of 355 quasars, only 6 circular polarization measurements were obtained in white light, and 21 using a broadband Bessell V-filter, for which the bandwidth is nevertheless not broad enough to average the circular polarization to almost zero.

Keeping the idea of averaging, we extended the model of magnetic field, by assuming a collection of cells of 100 kpc, with random 2 μG fields averaging to 0.3 μG, and letting most quantities fluctuate (size of cells, electron density, magnetic field). While these fluctuations can somewhat reduce the circular polarization, they also destroy the alignment which was the first reason to consider photon-pseudoscalar mixing.

Hence it seems that the combination of the alignments and of the absence of circular polarization remains at present a puzzle, which cannot be explained by photon-pseudoscalar mixing. One should note that this conclusion is based on the lack of circular polarization in 19 objects measured with the V-filter. It is of course possible that magnetic field configurations are special for these 19 objects, and some more data—or, equivalently, data in an even smaller bandwidth—may be needed to reach certainty. Note that, as we have discussed in Sec. II, similar conclusions hold in the case of a scalar ALP.

As a final note, the data on quasar polarization show that the polarizations are only typically a few percent. Photon-pseudoscalar mixing can be much more efficient than this at producing polarization. Hence the quasar data can be used to exclude part of the parameter space of ALPs. This will be the subject of a future paper [67].

ACKNOWLEDGMENTS

A. P. would like to thank Davide Mancusi for numerous discussions on technical issues, and Fredrik Sandin for his help about the use of the MPFR library. A. P. also thanks Javier Redondo for interesting exchanges about axion physics, as well as Cédric Lorcé, Diego Aristizabal, and Federico Ceccopieri for stimulating discussions. In addition, A. P. thanks Georg Raffelt who suggested what became the end of Sec. III B. D. H. is Senior Research Associate at F.R.S-FNRS; A. P. is an IISN researcher.

[18]Note also that considering another field should imply that it is coherent over angular distances even larger than the LSC scale: indeed, it should be located beyond it and still large enough so that light from angularly distant quasars passes through a field giving the same preferred direction.

APPENDIX A: PSEUDOSCALAR-PHOTON MIXING USING WAVE PACKETS

Here, we solve the system of Eq. (17) in the case of the steplike magnetic field presented in Sec. III A, using the decomposition of Eq. (18). Note that, as in the plane-wave case, we rephase $\phi(z, t)$ and use the gauge condition $A^0 = 0$, so that $\tilde{E}(z, \omega) = i\omega\tilde{A}(z, \omega)$.

The solutions in the first region are

$$E_I(z, t) = \int_{-\infty}^{\infty} d\omega\, e^{-i\omega t} i\omega [\tilde{A}_{i,I}(z = 0, \omega) e^{ik_E z} + \tilde{A}_{r,I}(z = 0, \omega) e^{-ik_E z}], \tag{A1}$$

$$\phi_I(z, t) = \int_{-\infty}^{\infty} d\omega\, e^{-i\omega t} [\tilde{\phi}_{i,I}(z = 0, \omega) e^{ik_\phi z} + \tilde{\phi}_{r,I}(z = 0, \omega) e^{-ik_\phi z}], \tag{A2}$$

with the dispersion relations $k_E = \sqrt{\omega^2 - {\omega_p}^2}$ and $k_\phi = \sqrt{\omega^2 - m^2}$. Here we have already used the fact that we will always consider amplitudes centered around ω_0, with $\omega_0 \gg \omega_p$, m, and decreasing sufficiently quickly with ω for the contributions from $\omega \leq \omega_p$, m to be negligible. Similarly, the solutions in the second region read

$$E_{II}(z, t) = \int_{-\infty}^{\infty} d\omega\, e^{-i\omega t} i\omega [\tilde{A}_{i,II}(z = 0, \omega)((c_{\rm mix})^2 e^{ik_C z} + (s_{\rm mix})^2 e^{ik_D z}) + \tilde{\phi}_{i,II}(z = 0, \omega) \frac{\sin(2\theta_{\rm mix})}{2} (e^{ik_C z} - e^{ik_D z})], \tag{A3}$$

$$\phi_{II}(z, t) = \int_{-\infty}^{\infty} d\omega\, e^{-i\omega t} [\tilde{A}_{i,II}(z = 0, \omega) \frac{\sin(2\theta_{\rm mix})}{2} (e^{ik_C z} - e^{ik_D z}) + \tilde{\phi}_{i,II}(z = 0, \omega)((s_{\rm mix})^2 e^{ik_C z} + (c_{\rm mix})^2 e^{ik_D z})], \tag{A4}$$

where k_C and k_D are respectively $k_+ = \sqrt{\omega^2 - {\mu_+}^2}$ and $k_- = \sqrt{\omega^2 - {\mu_-}^2}$ when $\omega_p > m$, and the other way around when $m > \omega_p$. As we are mostly interested in the small mixing case, the heaviest eigenmode of propagation is mostly made of the heaviest state among photons and pseudoscalars, and conversely for the lightest one. If $\mathcal{B}$ is set to zero, $k_C = k_E$ and $k_D = k_\phi$.

The amplitudes $\tilde{A}_{i,I}(0, \omega)$, $\tilde{A}_{r,I}(0, \omega)$, $\tilde{\phi}_{i,I}(0, \omega)$, $\tilde{\phi}_{r,I}(0, \omega)$, $\tilde{A}_{i,II}(0, \omega)$ and $\tilde{\phi}_{i,II}(0, \omega)$ are determined by initial and boundary conditions. They correspond to incident (i) or reflected (r) amplitudes that appear as light goes from region I into the potential barrier. To simplify our discussion, we now work in the case where there is no incident pseudoscalar flux in region I, namely $\phi_{i,I}(0, \omega) = 0$.

The continuity requirements on $E(z, t)$ and $\phi(z, t)$, and on their first derivatives with respect to z, at $z = 0$ then lead to relations where the only free parameter left is $\tilde{A}_{i,I}(z = 0, \omega)$. For completeness, they are

$$\tilde{A}_{i,II}(z = 0, \omega) = 2k_E \left[\frac{k_C (s_{\rm mix})^2 + k_D (c_{\rm mix})^2 + k_\phi}{k_E k_\phi + k_C k_D + k_E (k_C (s_{\rm mix})^2 + k_D (c_{\rm mix})^2 + k_\phi (k_C (c_{\rm mix})^2 + k_D (s_{\rm mix})^2)} \right] \tilde{A}_{i,I}(0, \omega) \equiv \mathcal{V} \tilde{A}_{i,I}(0, \omega), \tag{A5}$$

$$\tilde{\phi}_{i,II}(z = 0, \omega) = \tilde{\phi}_{r,I}(z = 0, \omega) = \left[\frac{k_E (k_C - k_D) \sin(2\theta_{\rm mix})}{k_E k_\phi + k_C k_D + k_E (k_C (s_{\rm mix})^2 + k_D (c_{\rm mix})^2) + k_\phi (k_C (c_{\rm mix})^2 + k_D (s_{\rm mix})^2)} \right] \tilde{A}_{i,I}(0, \omega) \equiv \mathcal{W} \tilde{A}_{i,I}(0, \omega), \tag{A6}$$

$$\tilde{A}_{r,I}(z = 0, \omega) = (\mathcal{V} - 1) \tilde{A}_{i,I}(0, \omega). \tag{A7}$$

In the case of an incident Gaussian wave packet

$$\tilde{E}_{i,I}(z = 0, \omega) = e^{-(a^2/4)(\omega - \omega_0)^2}, \tag{A8}$$

we obtain the following result for $E_{II}(z, t)$ (which is the only amplitude entering the expressions of the Stokes parameters in the second region):

$$E_{II}(z,t)=\int_{-\infty}^{\infty}d\omega\Big[\frac{\mathcal{V}-i\mathcal{W}}{4}\exp\Big(-\frac{a^2}{4}(\omega-\omega_0)^2+i(k_Cz-\omega t+2\theta_{\rm mix})\Big)$$
$$+\frac{\mathcal{V}+i\mathcal{W}}{4}\exp\Big(-\frac{a^2}{4}(\omega-\omega_0)^2+i(k_Cz-\omega t-2\theta_{\rm mix})\Big)+\frac{\mathcal{V}}{2}\exp\Big(-\frac{a^2}{4}(\omega-\omega_0)^2+i(k_Cz-\omega t)\Big)$$
$$-\frac{\mathcal{V}-i\mathcal{W}}{4}\exp\Big(-\frac{a^2}{4}(\omega-\omega_0)^2+i(k_Dz-\omega t+2\theta_{\rm mix})\Big)-\frac{\mathcal{V}+i\mathcal{W}}{4}\exp\Big(-\frac{a^2}{4}(\omega-\omega_0)^2+i(k_Dz-\omega t-2\theta_{\rm mix})\Big)$$
$$+\frac{\mathcal{V}}{2}\exp\Big(-\frac{a^2}{4}(\omega-\omega_0)^2+i(k_Dz-\omega t)\Big)\Big]; \tag{A9}$$

where $\mathcal{V}$, $\mathcal{W}$, k_C, k_D and $\theta_{\rm mix}$ are functions of ω. Note that if $g\mathcal{B}$ is set to zero, this reduces to

$$E_{II}(z,t;g\mathcal{B}=0)=E_\perp(z,t)=\int_{-\infty}^{\infty}d\omega\ \exp\Big(-\frac{a^2}{4}(\omega-\omega_0)^2+i(k_Ez-\omega t)\Big). \tag{A10}$$

We finally Taylor expand the coefficients and the arguments of the exponentials around ω_0 (up to the second order) to carry out the integrals (A9) and (A10) analytically to better than 1% for the case at hand (as was checked by estimating the contribution of the next order).

APPENDIX B: MIXING IN A MORE GENERAL MAGNETIC FIELD

Consider several regions with different magnetic fields, their direction and strength changing from one region to another. First of all, one can work out axion-photon mixing in a arbitrarily oriented transverse magnetic field $\vec{\mathcal{B}}=\mathcal{B}\cos\delta\vec{e}_1+\mathcal{B}\sin\delta\vec{e}_2$, where $\vec{e}_1$ and $\vec{e}_2$ are the basis vectors we will use throughout to keep track of an absolute direction and to define Stokes parameters.

We approximate $(\omega^2+\partial_z{}^2)\simeq 2\omega(\omega+i\partial_z)$ in the equations of motion for the fields, as the masses we use are indeed much smaller than the photon energies entering the problem. Inside a region, the system of equations reads

$$\left[\left(\omega+i\frac{\partial}{\partial z}\right)-\begin{pmatrix}\frac{{\omega_p}^2}{2\omega} & 0 & \frac{-g\mathcal{B}\cos\delta}{2}\\ 0 & \frac{{\omega_p}^2}{2\omega} & \frac{-g\mathcal{B}\sin\delta}{2}\\ \frac{-g\mathcal{B}\cos\delta}{2} & \frac{-g\mathcal{B}\sin\delta}{2} & \frac{m^2}{2\omega}\end{pmatrix}\right]\times\begin{pmatrix}A_1(z)\\ A_2(z)\\ \phi(z)\end{pmatrix}=0. \tag{B1}$$

We introduce $a_1(z)$, $a_2(z)$, and $\chi(z)$ such that we remove the $e^{i\omega z}$-dependence of the solutions:

$$\begin{pmatrix}A_1(z)\\ A_2(z)\\ \phi(z)\end{pmatrix}=\begin{pmatrix}a_1(z)\\ a_2(z)\\ \chi(z)\end{pmatrix}e^{i\omega z}, \tag{B2}$$

and then rotate by $(\frac{\pi}{2}-\delta)$ to an appropriate basis $(\vec{e}_\perp,\vec{e}_\parallel)$, such that $\vec{\mathcal{B}}=(0,\mathcal{B})$. Solving the equations in a way similar to the one used in Sec. II, and going back to the $(\vec{e}_1,\vec{e}_2)$ basis, we finally obtain:

$$\begin{pmatrix}a_1(z)\\ a_2(z)\\ \chi(z)\end{pmatrix}=\begin{pmatrix}K_{11} & K_{12} & K_{13}\\ K_{12} & K_{22} & K_{23}\\ K_{13} & K_{23} & K_{33}\end{pmatrix}\begin{pmatrix}a_1(0)\\ a_2(0)\\ \chi(0)\end{pmatrix} \tag{B3}$$

with

$$K_{11}=\sin^2\delta e^{-i({\omega_p}^2/2\omega)z}+\cos^2\delta((c_{\rm mix})^2e^{-i({\mu_C}^2/2\omega)z}+(s_{\rm mix})^2e^{-i({\mu_D}^2/2\omega)z}),$$
$$K_{22}=\cos^2\delta e^{-i({\omega_p}^2/2\omega)z}+\sin^2\delta((c_{\rm mix})^2e^{-i({\mu_C}^2/2\omega)z}+(s_{\rm mix})^2e^{-i({\mu_D}^2/2\omega)z}),$$
$$K_{12}=-\sin\delta\cos\delta e^{-i({\omega_p}^2/2\omega)z}+\cos\delta\sin\delta((c_{\rm mix})^2e^{-i({\mu_C}^2/2\omega)z}+(s_{\rm mix})^2e^{-i({\mu_D}^2/2\omega)z}),$$
$$K_{13}=\cos\delta\frac{\sin(2\theta_{\rm mix})}{2}(e^{-i({\mu_C}^2/2\omega)z}-e^{-i({\mu_D}^2/2\omega)z}),$$
$$K_{23}=\sin\delta\frac{\sin(2\theta_{\rm mix})}{2}(e^{-i({\mu_C}^2/2\omega)z}-e^{-i({\mu_D}^2/2\omega)z}),$$
$$K_{33}=(s_{\rm mix})^2e^{-i({\mu_C}^2/2\omega)z}+(c_{\rm mix})^2e^{-i({\mu_D}^2/2\omega)z}, \tag{B4}$$

where μ_C and μ_D are respectively μ_+ and μ_- when $\omega_p>m$, and the other way around when $m>\omega_p$.

When we consider light traveling through regions of different magnetic fields, we use this result inside each region, ensuring the continuity of the fields at the boundaries and neglecting reflected waves, which have an amplitude of order $(\frac{r_{\rm mix}}{\omega^2})$.

Note that for the ''patchy'' model, the magnetic field from cell to cell is not only rotated in the transverse plane, but can undergo the most general tridimensional rotation. As inside each region only the total transverse field is relevant, this gives lower transverse-field strengths. When we have allowed an additional underlying field, we have kept it in the $\vec{e}_2$ direction throughout and calculated the angle δ for each region.

[1] J. E. Kim, Phys. Rev. Lett. **43**, 103 (1979).
[2] M. A. Shifman, A. I. Vainshtein, and V. I. Zakharov, Nucl. Phys. **B166**, 493 (1980).
[3] A. R. Zhitnitsky, Sov. J. Nucl. Phys. **31**, 260 (1980).
[4] M. Dine, W. Fischler, and M. Srednicki, Phys. Lett. B **104**, 199 (1981).
[5] S. Weinberg, Phys. Rev. Lett. **40**, 223 (1978).
[6] F. Wilczek, Phys. Rev. Lett. **40**, 279 (1978).
[7] R. D. Peccei and H. R. Quinn, Phys. Rev. Lett. **38**, 1440 (1977).
[8] G. G. Raffelt, J. Phys. A **40**, 6607 (2007).
[9] J. Jaeckel and A. Ringwald, Annu. Rev. Nucl. Part. Sci. **60**, 405 (2010).
[10] P. Sikivie, Phys. Rev. Lett. **51**, 1415 (1983).
[11] G. Raffelt and L. Stodolsky, Phys. Rev. D **37**, 1237 (1988).
[12] A. De Angelis, M. Roncadelli, and O. Mansutti, Phys. Rev. D **76**, 121301 (2007).
[13] C. Burrage, A.-C. Davis, and D. J. Shaw, Phys. Rev. Lett. **102**, 201101 (2009).
[14] M. Fairbairn, T. Rashba, and S. V. Troitsky, arXiv:0901.4085.
[15] D. Hutsemékers, Astron. Astrophys. **332**, 410 (1998).
[16] D. Hutsemékers and H. Lamy, Astron. Astrophys. **367**, 381 (2001).
[17] P. Jain, G. Narain, and S. Sarala, Mon. Not. R. Astron. Soc. **347**, 394 (2004).
[18] D. Hutsemékers, R. Cabanac, H. Lamy, and D. Sluse, Astron. Astrophys. **441**, 915 (2005).
[19] R. Rusk and E. Seaquist, Astron. J. **90**, 30 (1985).
[20] S. A. Joshi *et al.*, Mon. Not. R. Astron. Soc. **380**, 162 (2007).
[21] B. Borguet, D. Hutsemékers, G. Letawe, Y. Letawe, and P. Magain, Astron. Astrophys. **478**, 321 (2008), and references therein.
[22] B. Borguet, D. Hutsemékers, G. Letawe, Y. Letawe, and P. Magain, in *Astronomical Polarimetry 2008: Science from Small to Large Telescopes*, edited by P. Bastien and N. Manset, ASP Conf. Series (2008) (to be published).
[23] P. Jain, S. Panda, and S. Sarala, Phys. Rev. D **66**, 085007 (2002).
[24] S. Das, P. Jain, J. P. Ralston, and R. Saha, J. Cosmol. Astropart. Phys. 06 (2005) 002.
[25] M. Y. Piotrovich, Y. N. Gnedin, and T. M. Natsvlishvili, arXiv:0805.3649.
[26] A. Payez, J. R. Cudell, and D. Hutsemékers, AIP Conf. Proc. **1038**, 211 (2008). A discussion on the implications of dichroism and birefringence is found in sections 3 and 4.
[27] D. Hutsemékers, A. Payez, R. Cabanac, H. Lamy, D. Sluse, B. Borguet, and J. R. Cudell, in *Astronomical Polarimetry 2008: Science from Small to Large Telescopes*, edited by P. Bastien and N. Manset, ASP Conf. Series (2008) (to be published).
[28] A. Payez, J. R. Cudell, and D. Hutsemékers, in *Proceedings of the 5th Patras Workshop on Axions, WIMPs and WISPs*, edited by J. Jaeckel, A. Lindner, and J. Redondo (Verlag Deutsches Elektronen-Synchrotron, Hamburg, (2009), p. 133.
[29] A. Payez, J. R. Cudell, and D. Hutsemékers, AIP Conf. Proc. **1241**, 444 (2010).
[30] A. Payez, D. Hutsemékers, and J. R. Cudell, AIP Conf. Proc. **1274**, 144 (2010).
[31] N. Agarwal, A. Kamal, and P. Jain, Phys. Rev. D **83**, 065014 (2011).
[32] D. Hutsemékers, B. Borguet, D. Sluse, R. Cabanac, and H. Lamy, Astron. Astrophys. **520**, L7 (2010).
[33] C. Biggio, E. Masso, and J. Redondo, Phys. Rev. D **79**, 015012 (2009). See discussion in section 2.
[34] P. W. Anderson, Phys. Rev. **130**, 439 (1963).
[35] E. D. Carlson and W. D. Garretson, Phys. Lett. B **336**, 431 (1994).
[36] C. Deffayet, D. Harari, J.-P. Uzan, and M. Zaldarriaga, Phys. Rev. D **66**, 043517 (2002).
[37] J. P. Vallee, Astron. J. **99**, 459 (1990).
[38] J. P. Vallee, Astron. J. **124**, 1322 (2002).
[39] M. Giovannini, Int. J. Mod. Phys. D **13**, 391 (2004).
[40] C. Burrage, A.-C. Davis, and D. J. Shaw, Phys. Rev. D **79**, 044028 (2009).
[41] J. P. Vallee, New Astron. Rev. **55**, 91 (2011).
[42] A. V. Kravtsov, A. A. Klypin, and Y. Hoffman, Astrophys. J. **571**, 563 (2002).
[43] H. S. Stockman, R. L. Moore, and J. R. P. Angel, Astrophys. J. **279**, 485 (1984).
[44] G. Berriman, G. D. Schmidt, S. C. West, and H. S. Stockman, Astrophys. J. Suppl. Ser. **74**, 869 (1990).
[45] D. Sluse, D. Hutsemékers, H. Lamy, R. Cabanac, and H. Quintana, Astron. Astrophys. **433**, 757 (2005).
[46] C. Csaki, N. Kaloper, and J. Terning, Phys. Lett. B **535**, 33 (2002).
[47] E. Mortsell, L. Bergstrom, and A. Goobar, Phys. Rev. D **66**, 047702 (2002).
[48] A. De Angelis, O. Mansutti, and M. Roncadelli, Phys. Lett. B **659**, 847 (2008).
[49] A. Mirizzi, G. G. Raffelt, and P. D. Serpico, Lect. Notes Phys. **741**, 115 (2008).
[50] D. Hutsemékers, H. Lamy, and M. Remy, Astron. Astrophys. **340**, 371 (1998).
[51] G. Schmidt and D. Hines, Astrophys. J. **512**, 125 (1999).
[52] H. Lamy and D. Hutsemékers, Astron. Astrophys. **427**, 107 (2004).
[53] L. Maiani, R. Petronzio, and E. Zavattini, Phys. Lett. B **175**, 359 (1986).
[54] R. Cameron *et al.*, Phys. Rev. D **47**, 3707 (1993).
[55] C. Sterken and J. Mandroid, *Astronomical Photometry—A Guide* (Kluwer Academic Publishers, Dordrecht, 1992).
[56] L. Monaco and C. Snodgrass, European Southern Observatory Report No. LSO-MAN-ESO-36100-0004, 2008.
[57] N. I. Shakura and R. A. Sunyaev, Astron. Astrophys. **24**, 337 (1973).
[58] C. S. Kochanek, X. Dai, C. Morgan, N. Morgan, S. Poindexter, and G. Chartas, in *Statistical Challenges in Modern Astronomy IV*, edited by G. J. Babu and E. D. Feigelson, ASP Conf. Series, Vol. 371 (2007), p. 43.
[59] A. Donges, Eur. J. Phys. **19**, 245 (1998).
[60] L. Frousse, G. Hanrot, V. Lefèvre, P. Pélissier, and P. Zimmermann, ACM Trans. Math. Softw. **33**, 15 (2007).
[61] J. D. Landstreet and J. R. P. Angel, Astrophys. J. **174**, L127 (1972).
[62] L. Stodolsky, Phys. Rev. D **58**, 036006 (1998).
[63] N. Bassan, A. Mirizzi, and M. Roncadelli, J. Cosmol. Astropart. Phys. 05 (2010) 010.

[64] K. Serkowski, Acta Astronomica **8**, 135 (1958). See Appendix A.

[65] K. Dolag, D. Grasso, V. Springel, and I. Tkachev, in *28th International Cosmic Ray Conference, ICRR* (University of Tokyo, Tokyo, 2003), pp. 735–738.

[66] K. Dolag, D. Grasso, V. Springel, and I. Tkachev, in *X-Ray and Radio Connections*, edited by L. Sjouwerman and K. Dyer (2004). Published electronically at http://www.aoc.nrao.edu/events/xraydio.

[67] A. Payez *et al.* (to be published).